iScience, Volume *23*

Supplemental Information

Degradation of Mutant Protein Aggregates within the Endoplasmic Reticulum of Vasopressin Neurons

Takashi Miyata, Daisuke Hagiwara, Yuichi Hodai, Tsutomu Miwata, Yohei Kawaguchi, Junki Kurimoto, Hajime Ozaki, Kazuki Mitsumoto, Hiroshi Takagi, Hidetaka Suga, Tomoko Kobayashi, Mariko Sugiyama, Takeshi Onoue, Yoshihiro Ito, Shintaro Iwama, Ryoichi Banno, Mami Matsumoto, Natsuko Kawakami, Nobuhiko Ohno, Hirotaka Sakamoto, and Hiroshi Arima

Supplemental Figures

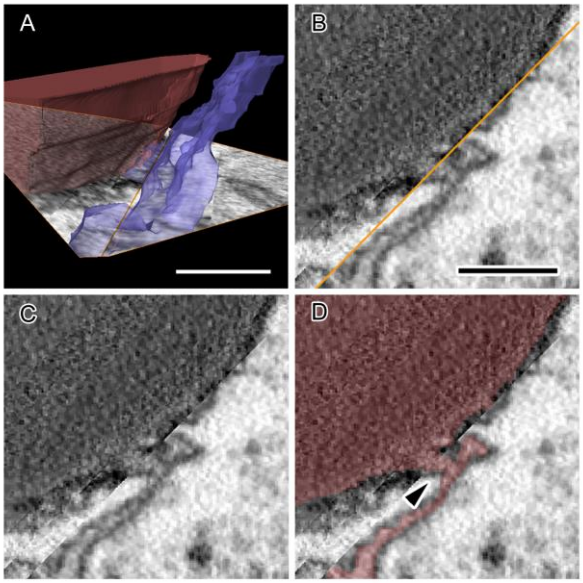

Figure S1. Luminal connections between ERACs and the intact ER in AVP neurons of FNDI mice, Related to Figure 2

The 3D reconstructed ERAC (A, red) and intact ER (A, blue) was cut at the plane of two angularly connected electron microscopic images (A) in order to observe the connection between an ERAC and the intact ER shown in Figure 2B. The cutting plane is shown as a montage image of the two angularly connected electron microscopic images (B-D), one of which corresponds to an obliquely cut slice montaged from the original SBF-SEM images. In the cutting plane image, the connecting line of the two electron microscopic images is shown as an orange line (B), and the luminal areas are colored red (D) to show the connection (D, arrow). Scale bars 500 nm.

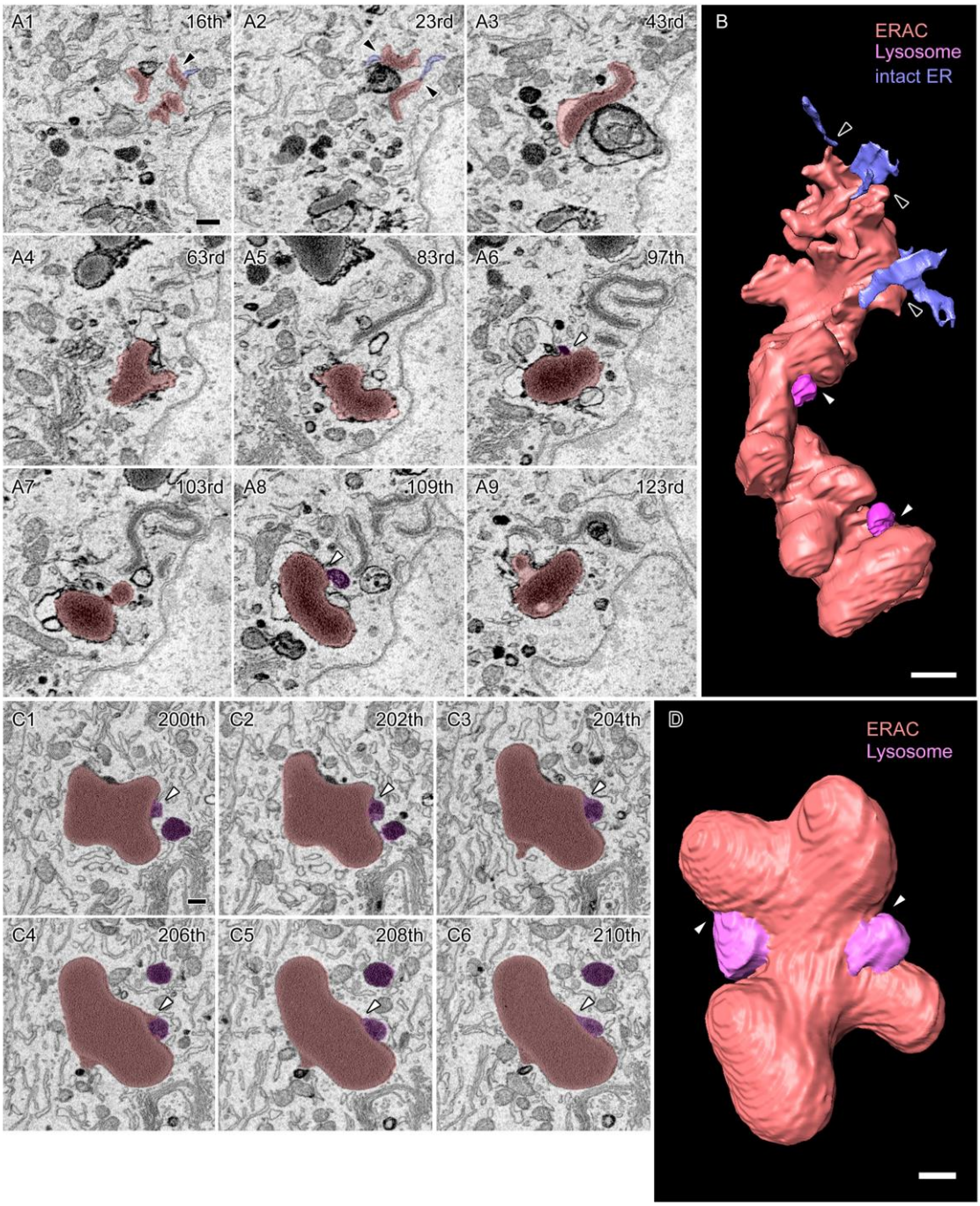
A1
16th
A2
23rd
A3
43rd
B
ERAC
Lysosome
intact ER
A4
63rd
A5
83rd
A6
97th
A7
103rd
A8
109th
A9
123rd
C1
200th
C2
202th
C3
204th
D
ERAC
Lysosome
C4
206th
C5
208th
C6
210th

Figure S2. An ERAC containing a relatively small amount of aggregates which fuses with lysosomes in AVP neurons of FNDI mice, Related to Figure 2

(A-D) Serial images of an ERAC containing a relatively small amount of aggregates (A1-9, red) and its 3D reconstruction (B) show connections (A1 and 2, arrowhead) with the intact ER (A1 and 2, blue) and the fusion (A6 and 8, white arrowheads) with lysosomes (A6 and 8, purple). Serial images of another ERAC containing a relatively small amount of aggregates (C1-6, red) and its 3D reconstruction (D) show the fusion (C1-6, white arrowheads) with a lysosome (C1-6, purple). The numbers in the upper-right corners show the respective slice number within the electron microscopic image stack. Scale bars: 500 nm. See also Videos S3 and 4.

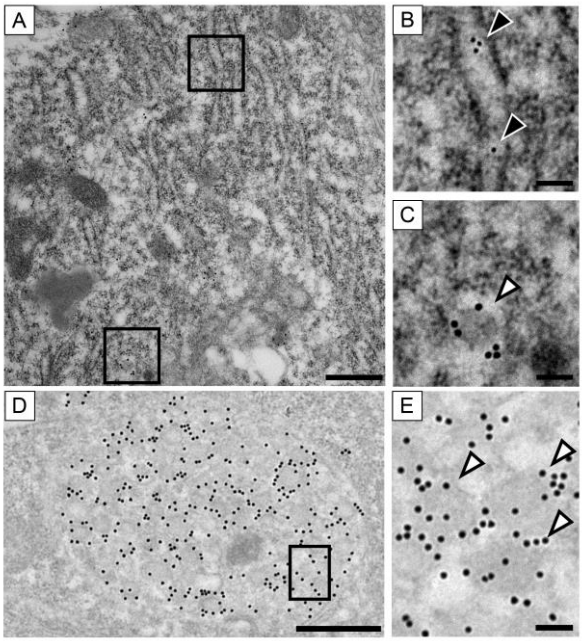

Figure S3. Ultrastructural localization of normal NPII and BiP in AVP neurons of wild-type mice, Related to Figures 3 and 4

(A-E) Immunoelectron microscopic analysis of BiP (10 nm gold particles, black arrowheads) and normal NPII (15 nm gold particles, white arrowheads) in AVP neurons of the SON (A-C) and in the posterior pituitary (D and E) of wild-type mice. BiP-immunoreactivity is associated with the membranous structures of rough ER (B) and normal NPII is found in neurosecretory vesicles (C). Higher magnification images of the boxed areas in A and D are shown in B, C, and E, respectively. Scale bars: 500 nm (A and D) and 100 nm (B, C, and E).

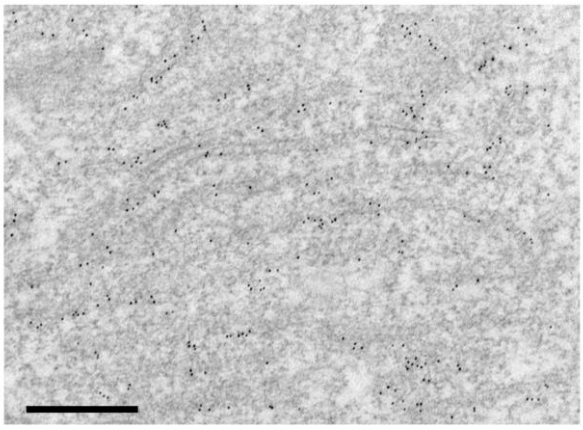

Figure S4. Ultrastructural localization of BiP in the intact ER in AVP neurons of FNDI mice, Related to Figure 4

Immunoelectron microscopic analysis for BiP (10 nm gold particles) in AVP neurons showed that BiP-immunoreactivity is associated with the membranous structures of rough ER in the SON of FNDI mice. Scale bars: 500 nm.

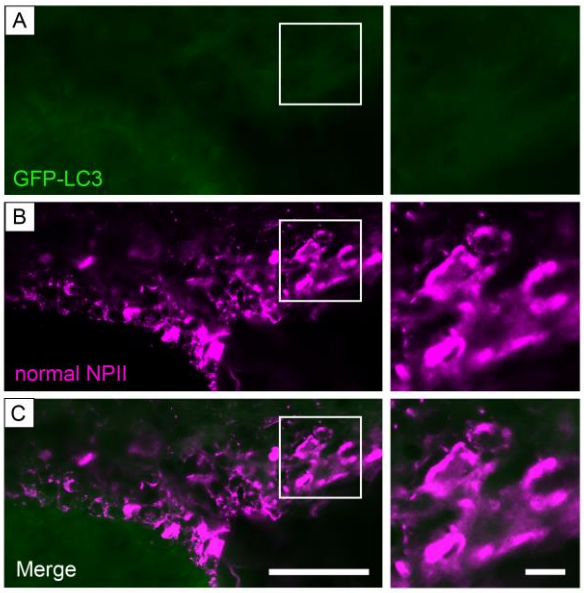

Figure S5. Localization of GFP in AVP neurons of GFP-LC3 mice, Related to Figure 4

(A-C) Immunofluorescence staining for GFP-LC3 (green) and normal NPII (magenta) in the SON of GFP-LC3 mice. Higher magnification images of the boxed areas in the left panels are shown at right. Scale bars: 50 μm (left panels) and 10 μm (right panels).

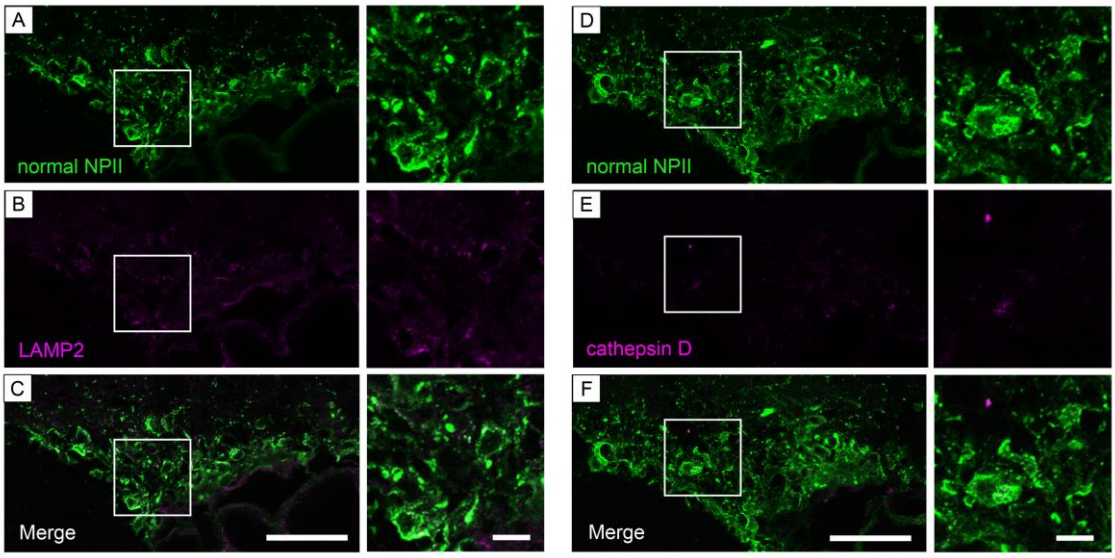

Figure S6. Localization of LAMP2 or cathepsin D in AVP neurons of wild-type mice, Related to Figure 5

(A-F) Immunofluorescence staining for normal NPII (green) and LAMP2 or cathepsin D (magenta) in the SON of wild-type mice. Higher magnification images of the boxed areas in the left panels are shown at right. Scale bars: 50 μm (left panels) and 10 μm (right panels).

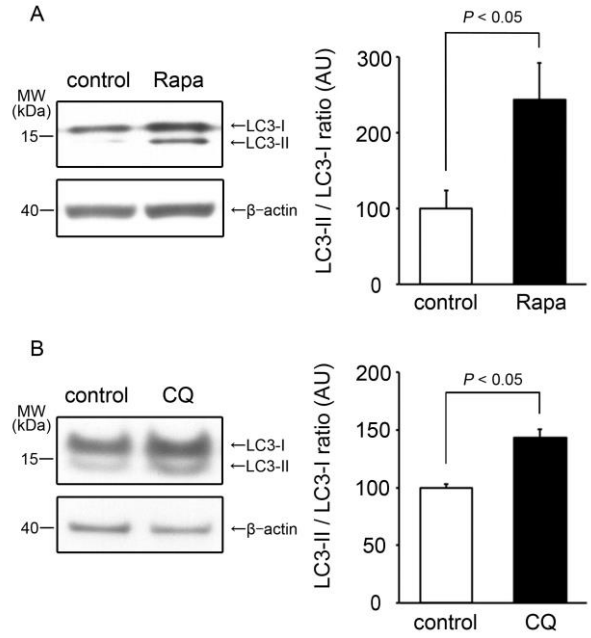

Figure S7. LC3 conversion (LC3-I to LC3-II) in the hypothalamus of wild-type mice treated with the autophagy inducer rapamycin or the lysosome inhibitor chloroquine, Related to Figure 6

(A and B) Representative immunoblot of protein lysates from the hypothalamus of wild-type mice in the control and rapamycin (Rapa, A) or chloroquine (CQ, B) groups immunolabeled for LC3. The adjacent bar graph displays the ratio of LC3II/LC3I densitometric signals relative to that of control mice. Results are expressed as means ± SE; n = 4 animals per group.

Transparent Methods

Animals

FNDI mice heterozygous for the mutant *Avp* gene (Cys98stop) were generated previously (Hayashi et al., 2009). All FNDI mice in the present study were backcrossed over 15 generations onto the C57BL/6J background. C57BL/6J mice were purchased from Chubu Science Materials (Nagoya, Japan). GFP-LC3 transgenic mice (strain GFP-LC3#53) harboring a rat LC3-enhanced GFP fusion construct under the control of the chicken β-actin promoter with the cytomegalovirus immediate early enhancer (Mizushima et al., 2004) were obtained from the RIKEN BioResource Center (Tsukuba, Japan). FNDI mice were crossed with GFP-LC3 transgenic mice to generate FNDI/GFP-LC3 mice. Mice were maintained under controlled conditions (23.0 ± 0.5°C, lights on 09:00 to 21:00), and male mice were used in the experiments. All procedures were approved by the Animal Experimentation Committee of the Nagoya University Graduate School of Medicine and performed in accordance with institutional guidelines for animal care and use.

Brain collection for immunohistochemistry

Three-month-old male FNDI mice, their wild-type littermates, FNDI/GFP-LC3 mice, and GFP-LC3 mice were deeply anesthetized and transcardially perfused with a cold fixative containing 4% paraformaldehyde (PFA) in 0.1 M phosphate buffer (pH 7.4). After fixation, brains were immediately removed and immersed in the same fixative for 3 h at 4°C. Brains were kept in PBS containing 10-20% sucrose at 4°C for cryoprotection. They were then embedded in Tissue-Tek O.C.T. compound (Sakura Finetechnical, Tokyo,

Japan) and stored at −80°C until sectioning. Brains were cut into 16-μm sections on a cryostat at −20°C, thaw-mounted on Superfrost Plus microscope slides (Matsunami Glass Ind., Osaka, Japan), and stored at −80°C until immunohistochemical analysis.

Antibodies

Primary antibodies used for immunofluorescence staining in the current study included: rabbit anti-mutant NPII (Cys98stop) (Hayashi et al., 2009), mouse anti-normal NPII (PS41; kindly provided by Dr. H Gainer, National Institutes of Health, Bethesda, MD, USA) (Ben-Barak et al., 1984; Ben-Barak et al., 1985), rabbit anti-BiP (#ab21685; Abcam, Cambridge, UK), rat anti-LAMP2 (#ab13524; Abcam), goat anti-cathepsin D (#sc6486; Santa Cruz Biotechnology, Dallas, TX, USA), and chicken anti-GFP (#ab13970; Abcam). The following secondary antibodies were used: Alexa Fluor 488-conjugated donkey anti-rabbit IgG (H+L) highly cross-adsorbed (#A-21206; Invitrogen, San Diego, CA, USA), Alexa Fluor 488-conjugated goat anti-chicken IgY (H+L) (#A-11039; Invitrogen), Alexa Fluor 488-conjugated donkey anti-mouse IgG (H+L) highly cross-adsorbed (#A-21202; Invitrogen), Alexa Fluor 546-conjugated donkey anti-mouse IgG (H+L) highly cross-adsorbed (#A-11036; Invitrogen), Alexa Fluor 546-conjugated F(ab')2-goat anti-rabbit IgG (H+L) cross-adsorbed (#A-11071; Invitrogen), Alexa Fluor 546-conjugated goat anti-rat IgG (H+L) cross-adsorbed (#A-11081; Invitrogen), and Alexa Fluor 546-conjugated donkey anti-goat IgG (H+L) cross-adsorbed (#A-11056; Invitrogen). Nuclei were stained with DAPI (#340-07971; DOJINDO, Kumamoto, Japan).

Immunohistochemistry

Frozen sections were washed with PBS for 15 min and then incubated with rabbit anti-

mutant NPII antibody (1:1000) in PBS with 0.3% Triton X-100 and 1% normal goat serum overnight at 4°C. After rinsing the sections with PBS, the primary antibody was probed using biotinylated goat anti-rabbit IgG (H+L) (1:200, #BA-1000; Vector Laboratories, Burlingame, CA, USA) for 3 h at room temperature. The sections were washed in PBS and then incubated with avidin-biotin complex solution (1:100, Vectastain ABC kit, #PK-4000; Vector Laboratories) for 90 min at room temperature before immersion in PBS containing 0.1% 3,3'-diaminobenzidine dihydrochloride (Sigma-Aldrich, St. Louis, MO, USA). Antibody-binding sites were visualized upon addition of 0.004% hydrogen peroxide. The number and diameter of inclusion bodies in the SON were measured using an Olympus DP73 digital camera system and an Olympus BX51 microscope equipped with cellSens Software (Olympus, Tokyo, Japan). The best-matched slices at 0.70 mm caudal from the bregma, according to the brain atlas [The Mouse Brain in Stereotaxic Coordinates, Academic Press, New York, 2000.], were selected from each mouse for analysis. The number of inclusion bodies per SON were counted, and the mean values for each mouse were subjected to statistical analyses. Five to seven mice per group were used for this analysis. For immunofluorescence staining, sections were incubated with these primary antibodies - rabbit anti-mutant NPII (1:1000), mouse anti-normal NPII (1:100), rat anti-LAMP2 (1:100), goat anti-cathepsin D (1:100) and chicken anti-GFP (1:10000) - overnight at 4 °C. The sections were then treated with a 1:1000 dilution of secondary antibodies for 1 h at room temperature. For double-immunofluorescence staining using the same host primary antibodies, rabbit anti-BiP and mutant NPII antibodies, sections were first incubated with rabbit anti-BiP antibody (1:600) overnight at 4°C and treated with Alexa Fluor 546-conjugated F(ab')2-goat anti-rabbit IgG (H+L) cross-adsorbed (1:100) for 1 h at room temperature. After washing in

PBS, the sections were next incubated with rabbit anti-mutant NPII antibody (1:2000) overnight at 4°C and treated with Alexa Fluor 488-conjugated donkey anti-rabbit IgG (H+L) highly cross-adsorbed (1:2000) for 1 h at room temperature. Fluorescence images were acquired with a laser-scanning confocal microscope (TiEA1R; Nikon Instech, Tokyo, Japan) or a fluorescence microscope (BZ-9000; Keyence, Osaka, Japan) and processed using Adobe Photoshop CS5 (Adobe Systems, San Jose, CA, USA). Three mice per experiment were used for the immunofluorescence analyses.

SBF-SEM

SBF-SEM analyses were performed as described previously with slight modifications (Matsumoto et al., 2019). Briefly, three-month-old male FNDI mice were deeply anesthetized and transcardially perfused with 4% PFA and 2.5% glutaraldehyde in 0.1 M phosphate buffer (pH 7.4). After fixation, brains were immediately removed and immersed overnight at 4°C in the same fixative. Brains were cut into 100-μm sections on a Vibratome (VT1200 S; Leica Biosystems, Wetzlar, Germany). Tissues were treated with 2% OsO_4 in 1.5% $K_4[Fe(CN)_6]$ for 1 h at 4°C, and subsequently 1% thiocarbohydrazide for 20 min, and 2% OsO_4 for 30 min at room temperature. Thereafter, the tissues were treated with 1% uranyl acetate at 4°C overnight and lead aspartate solution for 30 min at 65°C. The tissues were dehydrated in a graded series of ethanol (60, 80, 90, 95%), treated with dehydrated acetone, and embedded in Durcupan resin containing Ketjen black powder (5%) for 48 h at 60°C to ensure polymerization. SBF-SEM for the SON was performed using a SigmaVP scanning electron microscope (Carl Zeiss) equipped with a 3View in-chamber ultramicrotome system (Gatan). Serial image sequences were generated at 50-nm steps at a resolution of 4.8-5.7 nm per pixel. Sequential images were

processed with FIJI. Segmentation and three-dimensional reconstruction were performed using Microscopy Image Browser (http://mib.helsinki.fi) (Belevich et al., 2016) and Amira software (FEI Visualization Science Group, Hillsboro, OR, USA). Two mice were used for the SBF-SEM analyses.

Post-embedding immunoelectron microscopy

Three-month-old male FNDI mice, their wild-type littermates, and FNDI/GFP-LC3 mice were deeply anesthetized and transcardially perfused with 4% PFA and 0.1% glutaraldehyde in 0.1 M phosphate buffer (pH 7.4). Brains and neurohypophyses were immediately removed and immersed in the same fixative for 3 h at room temperature or overnight at 4ºC. Preparations were dehydrated through increasing concentrations of methanol, embedded in LR Gold resin (Electron Microscopy Sciences, PA, USA), and polymerized under UV lamps at –20ºC for 24 h. Ultrathin sections (70 nm in thickness) were collected on nickel grids coated with a collodion film, rinsed with PBS several times, then incubated with 2% normal goat serum and 2% BSA in 50 mM Tris(hydroxymethyl)-aminomethane-buffered saline (TBS; pH 8.2) for 30 min to block non-specific binding. The sections from FNDI mice were then incubated with either a 1:1,000 dilution of rabbit anti-mutant NPII antibody or a 1:60 dilution of rabbit anti-BiP antibody and a 1:200 dilution of mouse anti-normal NPII antibody (Castel et al., 1986) for 1 h at room temperature in the blocking solution. The sections were then washed with PBS, then incubated with a 1:50 dilution of a goat antibody against rabbit IgG conjugated to 10 nm gold particles (BBI Solutions, Cardiff, UK) and a goat antibody against mouse IgG conjugated to 15 nm gold particles (BBI Solutions) for 1 h at room temperature. The rat anti-LAMP2 antibody or the goat anti-cathepsin D antibody was also used both at 1:20

overnight at 4ºC in Can Get Signal Solution 1 (Toyobo, Tokyo, Japan). After the sections were washed with PBS, then incubated with a 1:50 dilution of either a goat antibody against rat IgG conjugated to 10 nm gold particles (Sigma, St. Louis, MO, USA) or a rabbit antibody against goat IgG conjugated to 10 nm gold particles (BBI Solutions) for 1 h at room temperature, respectively. To detect the GFP signals in tissues from FNDI/GFP-LC3 mice, the sections were incubated with a 1:20 dilution of rabbit anti-GFP antibody (Cell Signaling Technology Japan, Tokyo, Japan) for detection of GFP antigens to intensify the GFP-LC3 signal (for subcellular localization of LC3) for 1 h at room temperature. The immunoreactivity was detected with a streptavidin-biotin kit (Nichirei, Tokyo, Japan), followed by incubation with a 1:50 dilution of a goat antibody against horseradish peroxidase conjugated to 12 nm gold particles (Jackson ImmunoResearch Laboratory, PA, USA) for 1 h at room temperature. Finally, the sections were contrasted with uranyl acetate and lead citrate and viewed using an H-7650 (Hitachi, Tokyo, Japan) electron microscope operated at 80 kV. Three mice per experiment were used for the immunoelectron microscopic analyses.

Rapamycin and chloroquine administration

Two-month-old male FNDI mice and their wild-type littermates were divided into control and rapamycin or chloroquine groups. FNDI mice in the rapamycin or chloroquine groups were treated with an intraperitoneal administration of rapamycin (20 mg/kg/day, #R-5000, LC Laboratories, Woburn, MA, USA) or chloroquine (20 mg/kg/day, #C6628, Sigma-Aldrich) daily for 28 days, in addition to wild-type littermates for 7 days. The dosage of rapamycin or chloroquine employed in this study was determined based on previous studies (Cortes et al., 2012; Nalbandian et al., 2015;

Ravikumar et al., 2004; Vodicka et al., 2014; Zois et al., 2011).

Immunoblotting

The hypothalamus of wild-type mice were lysed in a buffer containing 10 mM Tris-HCl pH 7.4, 150 mM NaCl, 1% Triton X-100, 1% sodium deoxycholate, 0.1% SDS, 5 mM EDTA, 50 mM NaF, 2 mM Na_3VO_4, and 1% protease inhibitor cocktail (Sigma-Aldrich). After centrifuging the samples, protein concentrations in the supernatants were determined by bicinchoninic acid assay using a bicinchoninic acid kit (Sigma-Aldrich). Ten micrograms of protein per sample was separated by 10% SDS-PAGE and transferred to polyvinylidene difluoride membranes (Millipore). Blots were blocked in 5% skimmed milk in TBS-T solution (10 mM Tris-HCl pH 7.4, 150 mM NaCl and 0.1% Tween) for 1 h at RT. Membranes were incubated with a mouse anti-LC3 antibody (1:10000, #M186-3; Medical and Biological Laboratories, Nagoya, Japan) overnight at 4℃ and a rabbit anti-β-actin antibody (1:10000, #ab8227; Abcam) for 1 h at RT. Primary antibodies were probed with HRP-conjugated goat anti-mouse IgG (1:10000, #P0447; Agilent, Tokyo, Japan) and HRP-conjugated donkey anti-rabbit IgG (1:10000, #NA934; GE Healthcare, Little Chalfont, UK) for 1 h at RT. To improve sensitivity and the signal-to-noise ratio, Can Get Signal Immunoreaction Enhancer Solution (Toyobo) was used for the dilution of the primary and secondary antibodies. Immunoreactivity was detected using the ECL Prime Western Blotting Detection Reagent (GE Healthcare). Blots were quantified using NIH ImageJ software. Four mice per group were used for the immunoblotting analyses.

Statistical analysis

Statistical significance of the differences among groups was analyzed by an unpaired

t-test. Results are expressed as means ± SE, and differences were considered statistically significant at $P < 0.05$.

References

Belevich, I., Joensuu, M., Kumar, D., Vihinen, H., and Jokitalo, E. (2016). Microscopy Image Browser: A Platform for Segmentation and Analysis of Multidimensional Datasets. PLoS Biol *14*, e1002340.

Castel, M., Morris, J.F., Whitnall, M.H., and Sivan, N. (1986). Improved visualization of the immunoreactive hypothalamo-neurohypophysial system by use of immuno-gold techniques. Cell Tissue Res *243*, 193-204.

Cortes, C.J., Qin, K., Cook, J., Solanki, A., and Mastrianni, J.A. (2012). Rapamycin delays disease onset and prevents PrP plaque deposition in a mouse model of Gerstmann-Straussler-Scheinker disease. J Neurosci *32*, 12396-12405.

Matsumoto, M., Sawada, M., Garcia-Gonzalez, D., Herranz-Perez, V., Ogino, T., Bang Nguyen, H., Quynh Thai, T., Narita, K., Kumamoto, N., Ugawa, S.*, et al.* (2019). Dynamic Changes in Ultrastructure of the Primary Cilium in Migrating Neuroblasts in the Postnatal Brain. J Neurosci *39*, 9967-9988.

Nalbandian, A., Llewellyn, K.J., Nguyen, C., Yazdi, P.G., and Kimonis, V.E. (2015). Rapamycin and chloroquine: the in vitro and in vivo effects of autophagy-modifying drugs show promising results in valosin containing protein multisystem proteinopathy. PLoS One *10*, e0122888.

Ravikumar, B., Vacher, C., Berger, Z., Davies, J.E., Luo, S., Oroz, L.G., Scaravilli, F., Easton, D.F., Duden, R., O'Kane, C.J.*, et al.* (2004). Inhibition of mTOR induces autophagy and reduces toxicity of polyglutamine expansions in fly and mouse models of Huntington disease. Nat Genet *36*, 585-595.

Vodicka, P., Lim, J., Williams, D.T., Kegel, K.B., Chase, K., Park, H., Marchionini, D.,

Wilkinson, S., Mead, T., Birch, H.*, et al.* (2014). Assessment of chloroquine treatment for modulating autophagy flux in brain of WT and HD mice. J Huntingtons Dis *3*, 159-174.

Zois, C.E., Giatromanolaki, A., Sivridis, E., Papaiakovou, M., Kainulainen, H., and Koukourakis, M.I. (2011). "Autophagic flux" in normal mouse tissues: focus on endogenous LC3A processing. Autophagy *7*, 1371-1378.